RSC Advances

PAPER

View Article Online
View Journal | View Issue

Cite this: *RSC Adv.*, 2020, **10**, 43508

Improving ternary blend morphology by adding a conjugated molecule into non-fullerene polymer solar cells†

Di Zhao,‡[a] Pengcheng Jia,‡[a] Ling Li,‡[a] Yang Tang,‡[a] Qiuhong Cui,‡*[a] Chuanlang Zhan,‡*[b] Yanbing Hou,‡[a] Yufeng Hu,‡[a] Zhidong Lou‡[a] and Feng Teng‡*[a]

Received 22nd September 2020
Accepted 13th November 2020

DOI: 10.1039/d0ra08090j

rsc.li/rsc-advances

The use of ternary polymer solar cells (PSCs) is a promising strategy to enhance photovoltaic performance while improving the fill factor (FF) of a device, but is still a challenge due to the complicated morphology. Herein, ternary PSCs are fabricated *via* adding the conjugated small molecule ***p*-DTS(FBTTh$_2$)$_2$** into a well-known blended film, **PTB7-Th**:**IEICO-4F**. The ternary blend morphology and device characterization reveal that the addition of ***p*-DTS(FBTTh$_2$)$_2$** can improve crystallinity and optimize morphology, leading to the FF of the optimized device increasing to 73.69%. In combination with the advantages of an ultra-narrow bandgap material, **IEICO-4F**, with a broad optical absorption spectrum, the optimized ternary solar cell exhibits a high short-circuit current–density (J_{SC}) of 25.22 mA cm^{-2}. The best power conversion efficiency (PCE) is 12.84% for this optimized ternary device with 10 wt% ***p*-DTS(FBTTh$_2$)$_2$** in the donors. This work indicates that incorporating a small molecule with high crystallinity into host binary non-fullerene PSCs would give an active layer with high crystallinity, thus greatly enhancing the FFs and PCEs of PSCs.

Introduction

Polymer solar cells (PSCs) have achieved significant progress due to the rapid development of efficient organic semiconducting materials, especially for non-fullerene acceptor materials and polymer donor materials.[1–7] Compared with typical binary PSCs, ternary PSCs exhibit a strong potential for achieving a high power conversion efficiency (PCE), due to their superiority for expanding the absorption spectrum and improving photon collection.[8,9] Compared with tandem solar cells, the ternary system strategy exhibits not only improved photon harvesting by incorporating multiple organic materials but also because of the simplified fabrication technology.[8,9] In addition, incorporation of a third component leads to the optimization of exciton dissociation, charge carrier transport and collection.[8–10] However, the low crystallinity of conjugated polymers and the complicated morphology of the active layer would not be beneficial to achieve a high fill factor (FF) in ternary PSCs.

Recently, many strategies have been applied to improve the crystallinity of the blend film to obtain a device with a high FF, which is significantly associated with the body size, gradated bulk heterojunction (BHJ), π–π stacking distance, π–π stacking orientation, and domain purity.[11–14] The proper combination of small molecules and polymers provides a promising way to achieve high FF in ternary PSCs, due to the formation of nanostructures or alloy, together with a simultaneous enhancement in crystallinity.[13,14] Nevertheless, the addition of the third component may sacrifice the open-circuit voltage (V_{OC}), and new frontier orbitals (HOMO and LUMO) of the blend films would be formed because of the third component.[8,15,16] Therefore, it is important to select an appropriate third component with a suitable energy level. In addition, it is vital to adjust the content ratio in the active layer to attain smooth energy levels and optimize the film morphology for improving FF without sacrificing V_{OC}.

In this work, a well-known polymer donor **PTB7-Th** and a narrow bandgap non-fullerene acceptor **IEICO-4F** (chemical structures and normalized absorption as shown in Fig. 1a and b) have been used as host materials to fabricate binary PSCs, leading to a high short-circuit current–density.[17,18] A small molecular donor, 7,7′-(4,4-bis(2-ethylhexyl)-4*H*-silolo[3,2-b:4,5-b′]dithiophene-2,6-diyl)bis(6-fluoro-4-(5′-hexyl-[2,2′-bithiophen]-5-yl)benzo[*c*][1,2,5]thiadiazole), (***p*-DTS(FBTTh$_2$)$_2$**) which can improve the charge carrier mobility and the exciton dissociation and collection, was chosen as the third component to fabricate the ternary PSCs. The **PTB7-Th** molecular arrangement

[a]*Key Laboratory of Luminescence and Optical Information, Ministry of Education, Beijing Jiaotong University, Beijing, 100044, China. E-mail: qhcui@bjtu.edu.cn; fteng@bjtu.edu.cn*

[b]*Beijing National Laboratory for Molecular Sciences, CAS Key Laboratory of Photochemistry, Institute of Chemistry, Chinese Academy of Sciences, Beijing 100190, China. E-mail: clzhan@iccas.ac.cn*

† Electronic supplementary information (ESI) available. See DOI: 10.1039/d0ra08090j

‡ These authors contributed equally to this work.

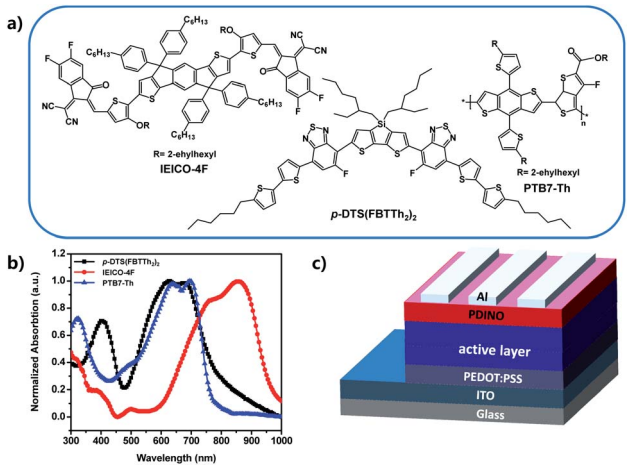

Fig. 1 (a) The chemical structures of IEICO-4F, *p*-DTS(FBTTh$_2$)$_2$, and PTB7-Th. (b) Normalized absorption spectra of neat PTB7-Th, *p*-DTS(FBTTh$_2$)$_2$, and IEICO-4F films. (c) The device structure of the PSC (glass/ITO/PEDOT:PSS/active layer/PDINO/Al).

and active layer phase separation can be optimized by incorporating the appropriate ratio of ***p*-DTS(FBTTh$_2$)$_2$** in donors, thereby enhancing the FF of ternary PSCs to 73.69%, and increasing the J_{SC} of the optimal device to 25.22 mA cm^{-2}. Because the HOMO difference between the molecular donor, ***p*-DTS(FBTTh$_2$)$_2$** and the polymer donor, **PBT7-Th** is very small (Fig. S1, ESI†), the V_{OC} is observed to reduce only slightly with the addition of ***p*-DTS(FBTTh$_2$)$_2$**. Combining the improved J_{SC} and FF, the optimized ternary PSCs reached 12.84% with 10 wt% ***p*-DTS(FBTTh$_2$)$_2$** in the donor molecule.

Results and discussion

A series of conventional PSCs were fabricated with the architecture of ITO/PEDOT:PSS/active layer/PDINO/Al (Fig. 1c). Fig. 2a illustrates the *J*–*V* (current density–voltage) curves of the PSCs with various contents of ***p*-DTS(FBTTh$_2$)$_2$** (0%, 10%, 20%, 30%), and Table 1 summarizes the principal photovoltaic parameters of the devices. The best PCE value of 12.84% was obtained for the ternary PSCs with 10 wt% of ***p*-DTS(FBTTh$_2$)$_2$**, and the other photovoltaic parameters were also improved

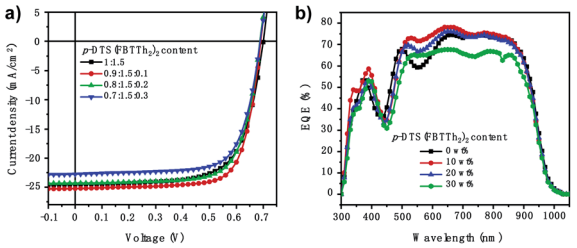

Fig. 2 (a) The *J*–*V* curves of PSCs with different *p*-DTS(FBTTh$_2$)$_2$ content levels. (b) The EQE spectra of the corresponding PSCs (calculated integrated current densities: 23.57 mA cm^{-2}, 24.46 mA cm^{-2}, 23.76 mA cm^{-2}, and 21.6 mA cm^{-2}).

Table 1 The device performances of PSCs with different ratios of *p*-DTS(FBTTh$_2$)$_2$

***p*-DTS(FBTTh$_2$)$_2$** content (wt%)	V_{OC} (V)	J_{sc} (mA cm^{-2})	FF (%)	Efficiency (%)
0 wt%	0.701	24.050	67.343	11.37
10 wt%	0.691	25.220	73.692	12.84
20 wt%	0.687	24.434	71.756	12.07
30 wt%	0.689	22.781	71.430	11.23

significantly, J_{SC} = 25.22 mA cm^{-2}, V_{OC} = 0.691 V, and FF = 73.69%.

Fig. 2a shows that the V_{OC} of the ternary devices is slightly reduced with the addition of ***p*-DTS(FBTTh$_2$)$_2$**, because the HOMO of ***p*-DTS(FBTTh$_2$)$_2$** was almost equal to that of **PTB7-Th**, as shown in Fig. S1 (ESI†). Compared with the binary device *J*–*V* curves, the series resistance (R_S) was reduced, and the shunt resistances (R_{SH}) were increased in the ternary device *J*–*V* curves, indicating that the FF of the ternary device was improved significantly with ***p*-DTS(FBTTh$_2$)$_2$** content. The FF was proved to be extremely dependent upon the R_S and R_{SH} of the devices, which was related to exciton dissociation and charge carrier recombination.[19] The improved FF showed that the addition of a small molecule could optimize exciton dissociation, suppress charge carrier recombination, and balance the carrier transport. Among the various ***p*-DTS(FBTTh$_2$)$_2$** content ratios, the FF of the ternary devices was the highest when the content of ***p*-DTS(FBTTh$_2$)$_2$** was 10 wt%, whereas the FF tended to decrease when the content of the small molecule was larger than 10 wt%. These results inferred that the addition of ***p*-DTS(FBTTh$_2$)$_2$** would regulate the crystallization condition of the blend film, and that the active layer may be destroyed by an excessive amount of the small molecule.

The J_{SC} was also improved with the addition of ***p*-DTS(FBTTh$_2$)$_2$**, and the calculated J_{SC} from the external quantum efficiency (EQE) spectra were approximately equal to the values measured from the *J*–*V* curves with a ~3% error, indicating that the results of the J_{SC} value were reliable. The EQE spectra of the optimized ternary PSCs were enhanced in the range from 300 nm to 400 nm, and 500 nm to 700 nm with the addition of ***p*-DTS(FBTTh$_2$)$_2$** (Fig. 2b), which coincided with the J_{SC} enhancement observed from the *J*–*V* curves. Compared with the absorption of the pure film, **PTB7-Th** (Fig. 1b), the EQE spectra at 350–450 nm mainly arose from the absorption of the polymer **PTB7-Th**, and therefore the enhanced EQE spectra indicated the enhanced molecular stacking of polymer **PTB7-Th** with the addition of ***p*-DTS(FBTTh$_2$)$_2$**. Moreover, an obvious red shift was seen in the range of 500–700 nm in the EQE spectra, as shown in Fig. 2b. With the increase of the content ratio of ***p*-DTS(FBTTh$_2$)$_2$**, the same effect was obtained in the absorption spectra of the ternary blend film (Fig. S2, ESI†), thus, indicating that the crystallinity of the blend film was enhanced with the addition of ***p*-DTS(FBTTh$_2$)$_2$**. This phenomenon was beneficial to the improvement of carrier mobility and collection efficiency, and therefore J_{SC} was increased. However, on continuously

increasing the ***p*-DTS(FBTTh$_2$)$_2$** content (>10%), both the EQE curves and the normalized absorption curves of the blend film showed a further red-shift and obvious decline, which may result from the morphology destruction or excess crystallization of the active layer.

To reveal the charge carrier transfer dynamic process in the binary and ternary blend films, the photoluminescence (PL) spectra of the **PTB7-Th:IEICO-4F** blend film with different ***p*-DTS(FBTTh$_2$)$_2$** contents were examined under 532 nm light excitation as shown in the results shown in Fig. S3a and b (ESI†). The **PTB7-Th:IEICO-4F** blend film results in extreme fluorescence quenching of **PTB7-Th**, and the PL emission intensity of the **PTB7-Th:IEICO-4F** blend film can be further quenched by adding a small ratio of ***p*-DTS(FBTTh$_2$)$_2$** into the blend films, indicating that the effective photoinduced charge transfer was promoted by adding ***p*-DTS(FBTTh$_2$)$_2$**. The effective photoinduced charge transfer was helpful for obtaining a higher J_{SC}.[19,20] In addition, as shown in Fig. S3 (ESI†), the PL emission intensity of the blend film with 10 wt% ***p*-DTS(FBTTh$_2$)$_2$** content was obviously quenched, which resulted in better phase separation. Subsequently, with the gradual addition of ***p*-DTS(FBTTh$_2$)$_2$**, the PL emission intensity increased slightly, which might be due to the enlarged domain size.

The electron-only devices ITO/TIPD (titanium(diisopropoxide) bis(2,4-pentanedionate))[21] active layer/PDINO/Al and hole-only devices ITO/PEDOT:PSS/active layer/Au were fabricated to further investigate the effect of the small molecule, ***p*-DTS(FBTTh$_2$)$_2$** on carrier transport and collection of ternary PSCs. Fig. 3a and b show the *J*–*V* curves of electron-only devices and hole-only devices under dark conditions.[22,23] The electron and hole mobilities of the devices with different contents were obtained by curve fitting based on the space charge limited current (SCLC) model.[22,23] Mobility was calculated according to the Mott–Gurney formula: $J = 9\varepsilon_r\varepsilon_0\mu_0V^2/8L^3$. Here, J is the current density, ε_r is the dielectric constant of the active layer, ε_0 is the dielectric constant in vacuum, μ_0 is the charge mobility of the blend film, V is the applied voltage, and L is the thickness of the active layer ($\approx$150 nm). The hole mobility (μ_h), electron mobility (μ_e), and the μ_h/μ_e ratios of the connected solar cells are presented in Table S1 (ESI†).[22,23] The electron and hole mobility of ternary polymer devices with small molecules were significantly improved, and the balance of hole mobility and electron mobility was achieved well in the devices with 10 wt% small molecule content (μ_h/μ_e = 1.12). The balanced carrier mobility was favorable for the transport of carriers in the organic solar cell, thus, imparting a high FF to the device.[11,24,25]

From further research the charge carrier transport and collection in the devices with different ratios of ***p*-DTS(FBTTh$_2$)$_2$**,[24,26] the dependence of V_{OC} on light intensity of the **PTB7-Th:IEICO-4F**-based binary and the ternary devices are shown in Fig. 3c. The recombination condition was obtained from: $V_{OC} \propto n(kT/q)\ln(P_{light})$, where k is the Boltzmann constant, T is the temperature (kelvin), and q is the elementary charge. The bimolecular recombination was the dominant process when the n value was close to 1, and the trap-assisted recombination was the primary process when the n value was close to 2.[27,28] The fitted n values were 1.184, 1.132, 1.296, and 1.223 for the devices with different contents of ***p*-DTS(FBTTh$_2$)$_2$**. It was observed that with the increase of the addition of ***p*-DTS(FBTTh$_2$)$_2$**, the n value of the device first decreased slightly and then increased gradually. According to Shockley–Read–Hall (SRH), it could be confirmed that the addition of an appropriate amount of small molecule ***p*-DTS(FBTTh$_2$)$_2$** could reduce the defect recombination in the device to some extent. Furthermore, the small molecule may aggregate to some extent as its content increases, resulting in the phase destruction in the blend film and the increased defect recombination in the solar cells.

To obtain more information on the performance improvement of optimized ternary devices, the photocurrent density *versus* effective voltage (J_{ph}–V_{eff}) curves were measured, as shown in Fig. 3d. Where, J_{ph} equals current density under illumination (J_L) minus current in the dark (J_D), *i.e.*, $J_{ph} = J_L - J_D$, V_{eff} equals the compensation voltage (V_0) minus the applied bias voltage (V_a), *i.e.*, $V_{eff} = V_0 - V_a$, and the V_0 is the voltage at J_{ph} = 0.[28] At high V_{eff}, photogenerated excitons were successfully obtained, and the free charge was collected by the electrode.[28] It was obvious that the J_{ph} of devices with the addition of ***p*-DTS(FBTTh$_2$)$_2$** reached the saturation state immediately at a relatively low V_{eff} (~0.3 V), thus indicating that the processes of exciton dissociation and charge carrier collection efficiency in ternary PSCs were very high. The processes of exciton dissociation and charge carrier collection that occurred in the active layer could be assessed by the values of J_{ph}/J_{sat} (J_{sat}, saturation current density). The J_{ph}/J_{sat} ratio of PSCs with different contents of ***p*-DTS(FBTTh$_2$)$_2$** under the conditions of short-circuit and maximum power output, was also calculated, as shown in Fig. 3d. Under the conditions of a short circuit, the J_{ph}/J_{sat} ratios were 97%, 97.2%, 96.8%, 95.9% for **PTB7-Th:IEICO-4F**, **PTB7-Th$_{(0.90)}$:*p*-DTS(FBTTh$_2$)$_{2(0.10)}$:IEICO-4F**, **PTB7-Th$_{(0.80)}$:*p*-DTS(FBTTh$_2$)$_{2(0.20)}$:IEICO-4F**, and **PTB7-Th$_{(0.70)}$:*p*-**

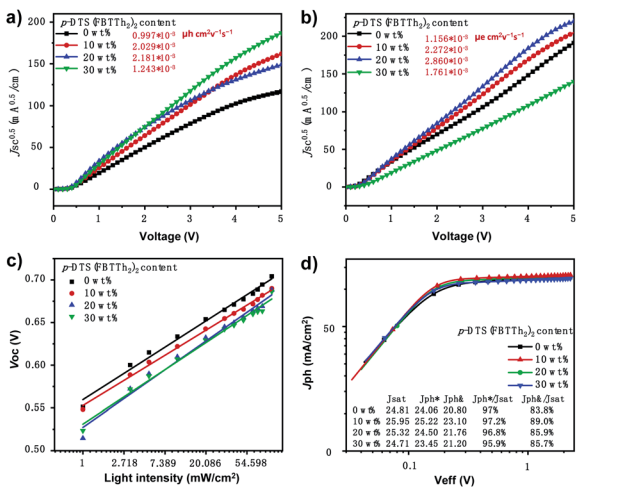

Fig. 3 *J*–*V* curves of (a) electron-only devices and (b) hole-only devices. (c) Curves showing V_{OC} dependence on light illumination intensity of the binary and optimized ternary PSCs. (d) J_{ph}–V_{eff} curves of typical PSCs.

DTS(FBTTh$_2$)$_{2(0.30)}$:IEICO-4F, respectively, which indicated that both binary and ternary devices demonstrated excellent exciton dissociation efficiency.[28]

Under the conditions of maximum power, the J_{ph}/J_{sat} ratios were 83.8%, 89.0%, 85.9%, 85.7% for **PTB7-Th:IEICO-4F**, **PTB7-Th$_{(0.90)}$:*p*-DTS(FBTTh$_2$)$_{2(0.10)}$:IEICO-4F**, **PTB7-Th$_{(0.80)}$:*p*-DTS(FBTTh$_2$)$_{2(0.20)}$:IEICO-4F**, and **PTB7-Th$_{(0.70)}$:*p*-DTS(FBTTh$_2$)$_{2(0.30)}$:IEICO-4F**, respectively, indicating that the optimized ternary solar cells (***p*-DTS(FBTTh$_2$)$_2$** 10 wt%) demonstrated a higher charge carrier collection efficiency and lower charge carrier recombination than the binary device. For the moment, the tendency of the J_{ph}/J_{sat} ratio to decrease coincided with that of the FF. In addition, the decreased series resistances and the increased shunt resistances of the optimized ternary solar cells from the *J*–*V* curve with the 10 wt% of ***p*-DTS(FBTTh$_2$)$_2$** indicated that there was a better contact between the active layer and electrodes which was beneficial to the charge carrier collection.

It is well-known that the performance of the device is deeply impacted by the degree of phase separation of the blend film, which strongly influenced the exciton dissociation, charge transport, and collection in the device.[24,29] To further investigate the influence of ***p*-DTS(FBTTh$_2$)$_2$** on the phase separation of the active layer, atomic force microscopy (AFM) and transmission electron microscopy (TEM) analyses were carried out. The treatment condition of binary and ternary blend films was the same as that of the blend films of the devices. The height and phase images of **PTB7-Th:IEICO-4F**, **PTB7-Th$_{(0.90)}$:*p*-DTS(FBTTh$_2$)$_{2(0.10)}$:IEICO-4F**, **PTB7-Th$_{(0.80)}$:*p*-DTS(FBTTh$_2$)$_{2(0.20)}$:IEICO-4F**, and **PTB7-Th$_{(0.70)}$:*p*-DTS(FBTTh$_2$)$_{2(0.30)}$:IEICO-4F** blend films are shown in Fig. 4. According to the height images, the statistical average data root-mean-square (RMS) roughness of films are 6.15, 4.05, 5.01, and 5.91 nm, respectively. This indicated that the optimal compatibility and the smoothest surface were obtained with 10 wt% ***p*-DTS(FBTTh$_2$)$_2$**. The AFM phase images of the active layers also show the optimized degree of phase separation and domain size with the 10 wt% of ***p*-DTS(FBTTh$_2$)$_2$**, which was favorable for exciton dissociation, charge carrier transport, and charge collection, with correspondingly enhanced J_{SC} and FF. With continuous enhancements to the ***p*-DTS(FBTTh$_2$)$_2$** content, the surface roughness was noted to increase due to the aggregation of small molecules and then excessively crystallized, which was also consistent with the decrease of J_{SC} and FF. The TEM images are shown in Fig. 5, and the bright and dark regions in the images correspond to the donor and acceptor regions, respectively. A small proportion of the small molecule, ***p*-DTS(FBTTh$_2$)$_2$** was incorporated into the blend film, and the degree of phase separation of the ternary blend film was not

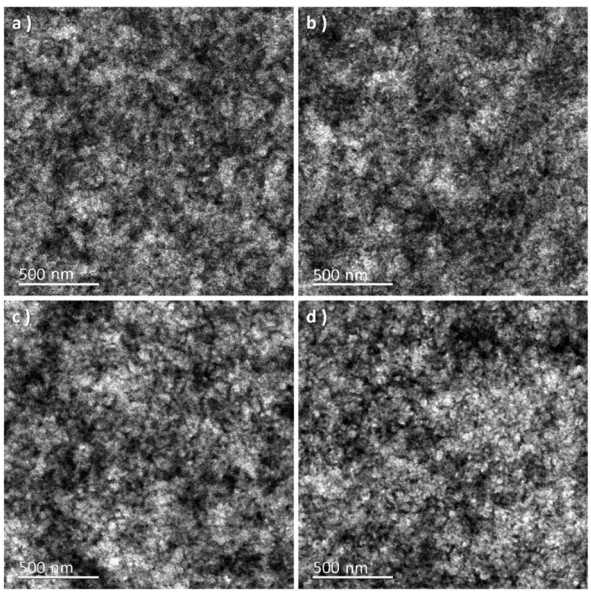

Fig. 5 TEM images showing the effects of different ***p*-DTS(FBTTh$_2$)$_2$** content levels.

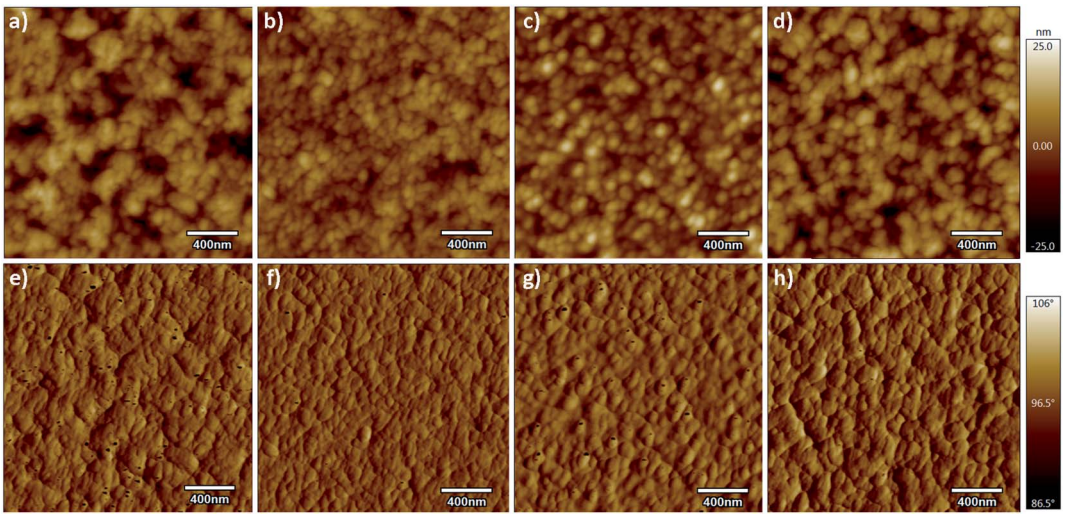

Fig. 4 AFM surface morphology height (upper) and phase (lower) images at different ***p*-DTS(FBTTh$_2$)$_2$** content levels (RMS: 6.15, 4.05, 5.01, and 6.88).

significantly changed. However, when the ***p*-DTS(FBTTh$_2$)$_2$** content of the small molecule was 20 wt% or more, the morphology of the ternary blend film deteriorated unmistakably, and the unfavorable rough fibrillary structure even formed inside the films. This indicated that the degree of phase separation was destroyed, which was due to the accumulative crystallization of excessive ***p*-DTS(FBTTh$_2$)$_2$**.[14,30] Thus, the moderate addition of ***p*-DTS(FBTTh$_2$)$_2$** could enhance the crystallinity of the films, which conformed to the normalized absorption of blend films, as Fig. S2 (ESI†) shows.

Conclusions

To summarize, highly efficient ternary polymer solar cells were designed and fabricated *via* combining the highly crystalline small molecule ***p*-DTS(FBTTh$_2$)$_2$** and ultra-narrow bandgap non-fullerene acceptor **IEICO-4F**. The ternary device with 10 wt% ***p*-DTS(FBTTh$_2$)$_2$** shows an extremely high J_{SC} of 25.22 mA cm^{-2} due to the ultra-narrow bandgap caused by its broad optical absorption spectrum. Furthermore, a high FF of 73.69% is also obtained due to the better phase separation and crystallinity, which gives efficient exciton dissociation and charge transport. At the same time, the selected energy level reduced the V_{OC} of the ternary devices slightly compared to the binary device. This work shows that the matching of a third component with good crystallinity and a proper energy level with the host system can be used for obtaining high-efficiency ternary PSCs.

Experimental

Device fabrication

The **PTB7-Th** and ***p*-DTS(FBTTh$_2$)$_2$** were procured from the 1-Material company (Canada). The Baytron Clevios P VP AI 4083 (PEDOT:PSS, Heraeus Group, Germany) was imported by the Solarmer. The electron transporting materials (ETM), *N*,*N*-bis(3,3-dimethyl-3-amino *N*-oxide-*n*-propyl) perylene diimide (PDINO)[31] and **IEICO-4F** were purchased from Solarmer. The device was fabricated by constructing the ITO/PEDOT:PSS/active layers/PDINO/Al, and the device structure is shown in Fig. 1c. The ITO glasses were cleaned with detergent, deionised water, acetone, and isopropanol for 20 min at each step. After drying under nitrogen gas, the ITO glasses were treated with ultraviolet/ozone for 20 min. Then, the hole transport layer, PEDOT:PSS was prepared on the cleaned ITO glasses at 6000 revolutions per minute (rpm). Then, the PEDOT:PSS substrates were immediately annealed at 150 °C for 20 min. The **PTB7-Th:*p*-DTS(FBTTh$_2$)$_2$:IEICO-4F** blends with different weight ratios (1 : 0:1.5, 0.9 : 0.1 : 1.5, 0.8 : 0.2 : 1.5, 0.7 : 0.3 : 1.5) were dissolved in chlorobenzene (with the polymer maintained at a concentration of 10 mg mL^{-1}). Then, all these solutions were placed on a thermostatically heated magnetic stirrer at 50 °C for 10 h. Next, 4% (volume fraction) of 1-chloronaphthalene (CN) was added into all these solutions. The active layer was spin-coated on to the PEDOT:PSS substrates at 1800 rpm for 30 s. Then the active layer was thermally annealed for 10 min on the thermostat at 80 °C, and the optimal thickness of active layer was about 150 nm. Then, the PDINO was spin-coated on to the active layer at 3000 rpm for 30 s. The electron transporting layer, PDINO (1.0 mg mL^{-1} in methanol) was fabricated by dynamic spin-coating (with the spin coater kept at 3000 rpm and then the solution was dropped on to the active layer) to avoid virtual high J_{SC} of the PSCs.[32] Finally, the Al electrodes (*ca.* 80 nm, under a vacuum of 10^{-4} Pa) were deposited on the top of the devices.

Film and device characterization

The *J*–*V* characteristics of all the binary and ternary polymer solar cells were measured using a 2400 source meter (Keithley). The performance of all the devices was conducted under AM 1.5G (irradiated at 100 mW cm^{-2} using a reference silicon cell). The EQE was measured under air using a QE-R3011 instrument (Enli, Taiwan). The UV-Vis absorption spectra of the spin-coated neat films as well as the blend films were obtained using a U-3010 UV-Vis spectrophotometer (Hitachi). Cyclic voltammetry (C–V) measurements were obtained using a CHI 660 electrochemical workstation (CH Instruments) with a glassy carbon electrode as working electrode, a Pt wire as the counter electrode, and a Ag/AgCl reference electrode. The AFM images were obtained using a Cypher S AFM (Oxford Instruments). The transmission electron microscopy (TEM) images of the blend films were recorded using a JEM-1400 TEM (Jeol) operated at 80 kV.

Conflicts of interest

There are no conflicts to declare.

Acknowledgements

This work was supported by the National Natural Science Foundation of China (51603010, 61875009, 91433202) and the Fund of Ministry of Education of China (2018JBM068).

Notes and references

1 J. Hou, O. Inganäs, R. H. Friend and F. Gao, *Nat. Mater.*, 2018, **17**, 119–128.
2 C. Yan, S. Barlow, Z. Wang, H. Yan, A. K.-Y. Jen, S. R. Marder and X. Zhan, *Nat. Rev. Mater.*, 2018, **3**, 1–19.
3 P. Cheng, G. Li, X. Zhan and Y. Yang, *Nat. Photonics*, 2018, **12**, 131–142.
4 A. Wadsworth, M. Moser, A. Marks, M. S. Little, N. Gasparini, C. J. Brabec, D. Baran and I. McCulloch, *Chem. Soc. Rev.*, 2019, **48**, 1596–1625.
5 J. Yuan, Y. Zhang, L. Zhou, G. Zhang, H.-L. Yip, T.-K. Lau, X. Lu, C. Zhu, H. Peng and P. A. Johnson, *Joule*, 2019, **3**, 1140–1151.
6 K. Jiang, Q. Wei, J. Y. L. Lai, Z. Peng, H. K. Kim, J. Yuan, L. Ye, H. Ade, Y. Zou and H. Yan, *Joule*, 2019, **3**, 3020–3033.
7 H. Fu, Z. Wang and Y. Sun, *Angew. Chem., Int. Ed.*, 2019, **58**, 4442–4453.
8 Q. An, F. Zhang, J. Zhang, W. Tang, Z. Deng and B. Hu, *Energy Environ. Sci.*, 2016, **9**, 281–322.

9 L. Lu, M. A. Kelly, W. You and L. Yu, *Nat. Photonics*, 2015, **9**, 491–500.
10 N. Gasparini, A. Salleo, I. McCulloch and D. Baran, *Nat. Rev. Mater.*, 2019, **4**, 229–242.
11 M.-H. Jao, H.-C. Liao and W.-F. Su, *J. Mater. Chem. A*, 2016, **4**, 5784–5801.
12 G. Zhang, K. Zhang, Q. Yin, X.-F. Jiang, Z. Wang, J. Xin, W. Ma, H. Yan, F. Huang and Y. Cao, *J. Am. Chem. Soc.*, 2017, **139**, 2387–2395.
13 Y. Zhang, D. Deng, K. Lu, J. Zhang, B. Xia, Y. Zhao, J. Fang and Z. Wei, *Adv. Mater.*, 2015, **27**, 1071–1076.
14 J. Zhang, Y. Zhang, J. Fang, K. Lu, Z. Wang, W. Ma and Z. Wei, *J. Am. Chem. Soc.*, 2015, **137**, 8176–8183.
15 H. Li, Z.-G. Zhang, Y. Li and J. Wang, *Appl. Phys. Lett.*, 2012, **101**, 163302.
16 Q. An, F. Zhang, X. Yin, Q. Sun, M. Zhang, J. Zhang, W. Tang and Z. Deng, *Nano Energy*, 2016, **30**, 276–282.
17 H. Yao, Y. Cui, R. Yu, B. Gao, H. Zhang and J. Hou, *Angew. Chem., Int. Ed.*, 2017, **56**, 3045–3049.
18 X. Song, N. Gasparini, L. Ye, H. Yao, J. Hou, H. Ade and D. Baran, *ACS Energy Lett.*, 2018, **3**, 669–676.
19 Q. An, F. Zhang, L. Li, J. Wang, Q. Sun, J. Zhang, W. Tang and Z. Deng, *ACS Appl. Mater. Interfaces*, 2015, **7**, 3691–3698.
20 Y. Lin, J. Wang, Z. G. Zhang, H. Bai, Y. Li, D. Zhu and X. Zhan, *Adv. Mater.*, 2015, **27**, 1170–1174.
21 Z. a. Tan, W. Zhang, Z. Zhang, D. Qian, Y. Huang, J. Hou and Y. Li, *Adv. Mater.*, 2012, **24**, 1476–1481.
22 M.-A. Pan, T.-K. Lau, Y. Tang, Y.-C. Wu, T. Liu, K. Li, M.-C. Chen, X. Lu, W. Ma and C. Zhan, *J. Mater. Chem. A*, 2019, **7**, 20713–20722.
23 Y. Chang, T.-K. Lau, M.-A. Pan, X. Lu, H. Yan and C. Zhan, *Mater. Horiz.*, 2019, **6**, 2094–2102.
24 Q. An, F. Zhang, Q. Sun, J. Wang, L. Li, J. Zhang, W. Tang and Z. Deng, *J. Mater. Chem. A*, 2015, **3**, 16653–16662.
25 N. Gasparini, X. Jiao, T. Heumueller, D. Baran, G. J. Matt, S. Fladischer, E. Spiecker, H. Ade, C. J. Brabec and T. Ameri, *Nat. Energy*, 2016, **1**, 1–9.
26 X. Huang, L. Lv, Y. Hu, Z. Lou, Y. Hou and F. Teng, *Org. Electron.*, 2017, **42**, 107–114.
27 A. Zeng, M. Pan, B. Lin, T.-K. Lau, M. Qin, K. Li, W. Ma, X. Lu, C. Zhan and H. Yan, *Sol. RRL*, 2020, **4**, 1900353.
28 Q. An, F. Zhang, Q. Sun, M. Zhang, J. Zhang, W. Tang, X. Yin and Z. Deng, *Nano Energy*, 2016, **26**, 180–191.
29 Z. Hu, J. Wang, Z. Wang, W. Gao, Q. An, M. Zhang, X. Ma, J. Wang, J. Miao and C. Yang, *Nano Energy*, 2019, **55**, 424–432.
30 J. A. Love, C. M. Proctor, J. Liu, C. J. Takacs, A. Sharenko, T. S. Van Der Poll, A. J. Heeger, G. C. Bazan and T. Q. Nguyen, *Adv. Funct. Mater.*, 2013, **23**, 5019–5026.
31 Z.-G. Zhang, B. Qi, Z. Jin, D. Chi, Z. Qi, Y. Li and J. Wang, *Energy Environ. Sci.*, 2014, **7**, 1966–1973.
32 J. Gao, Q. An, M. Zhang, J. Miao, X. Ma, Z. Hu, J. Wang and F. Zhang, *Phys. Chem. Chem. Phys.*, 2019, **21**, 5790–5795.